Electronic Supplementary Information

A new strategy to synthesize three-coordinate mononuclear copper(I) halide complexes containing bulky terphenyl bidentate phosphine ligand and their luminescent properties

Li-Ping Liu, Rui Zhang, Li Liu*, Xin-Xin Zhong*, Fa-Bao Li, Lei Wang*, Wai-Yeung Wong*, Guang-Hua Li, Heng-Jiang Cong*, Njud S. Alharbi, Yi Zhao

Contents

Experimental Details

Experimental Details

1. NMR Experiments

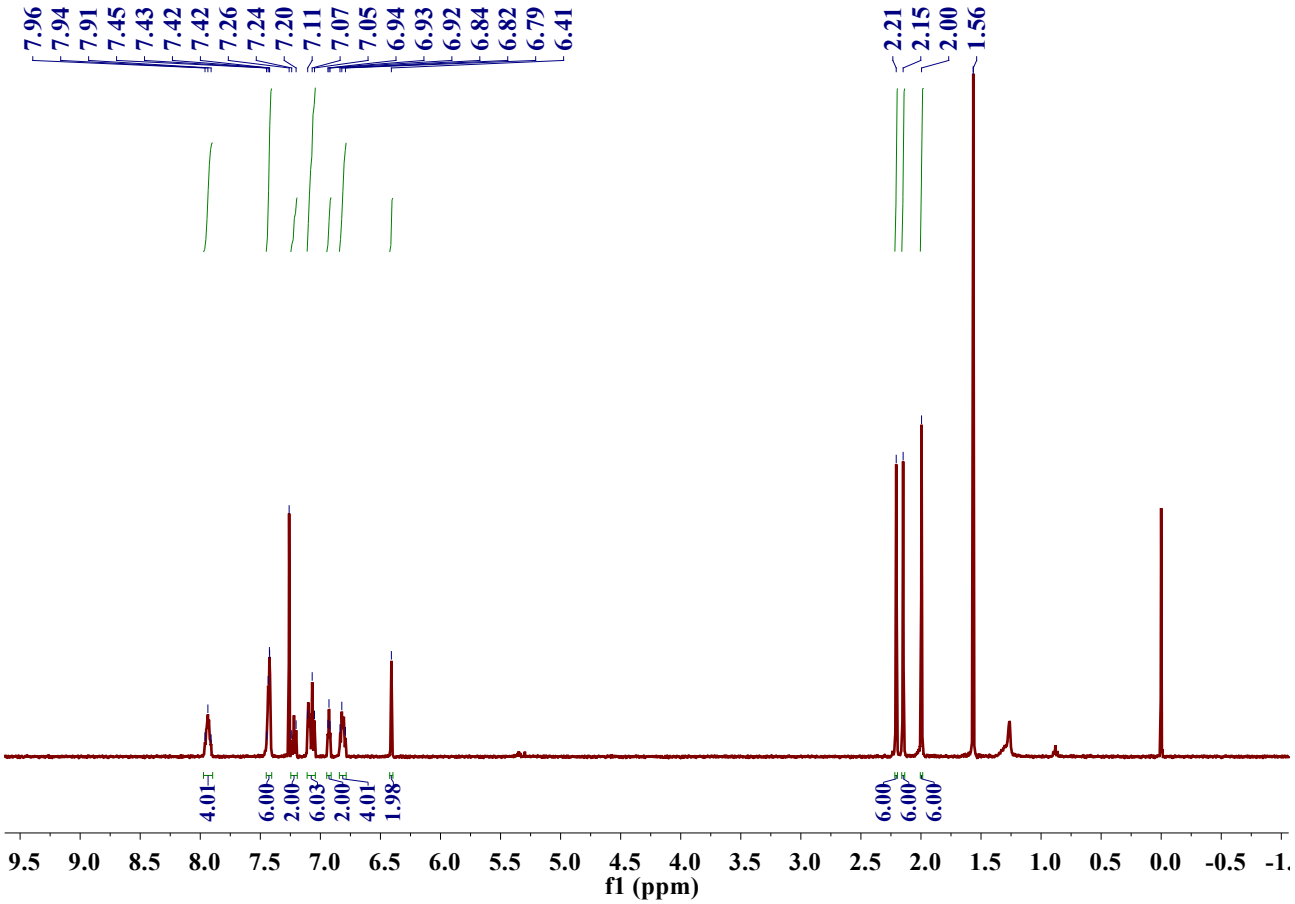

Fig. S1. ^{1}H NMR spectrum of **1** in $CDCl_3$.

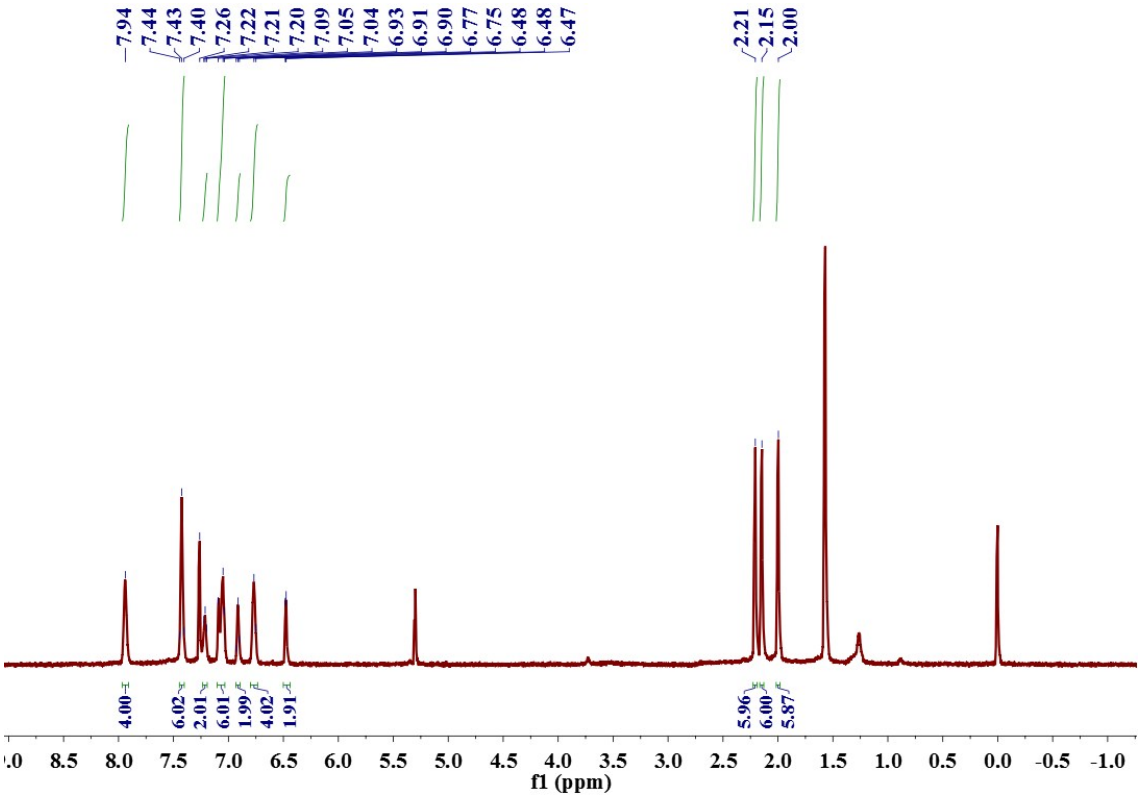

Fig. S2. ^{1}H NMR spectrum of **2** in $CDCl_3$.

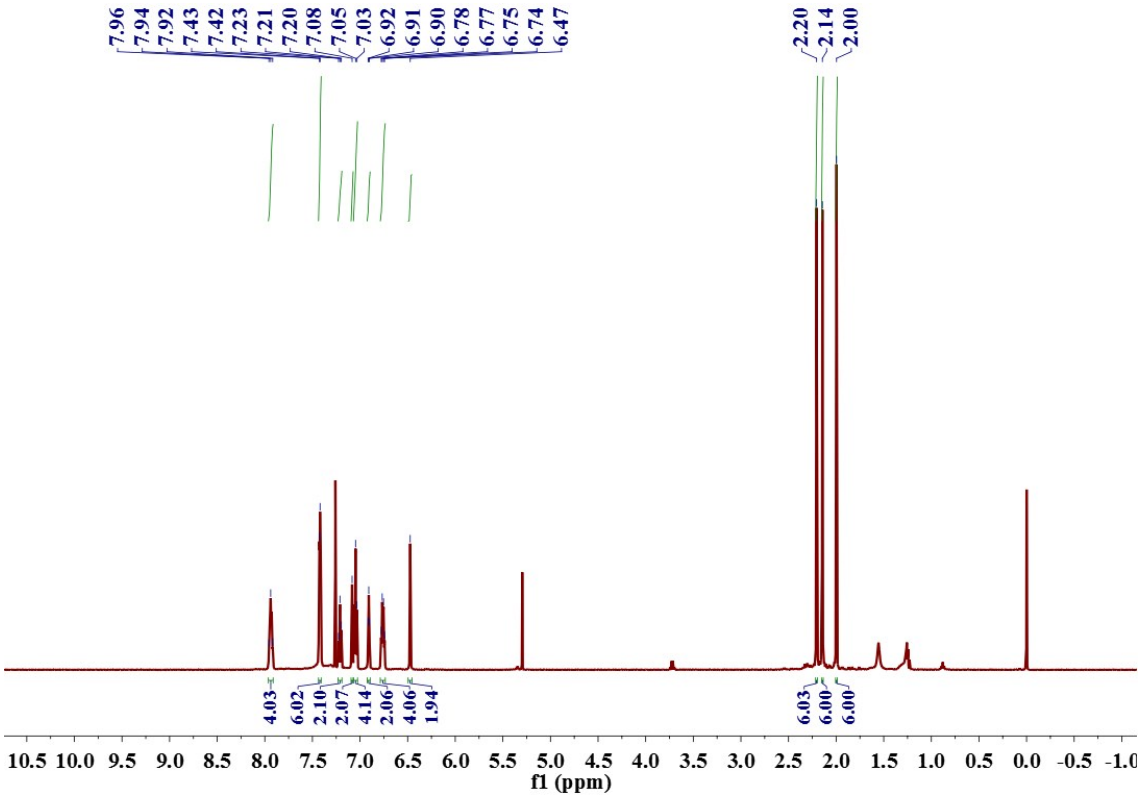

Fig. S3. ^{1}H NMR spectrum of **3** in $CDCl_3$.

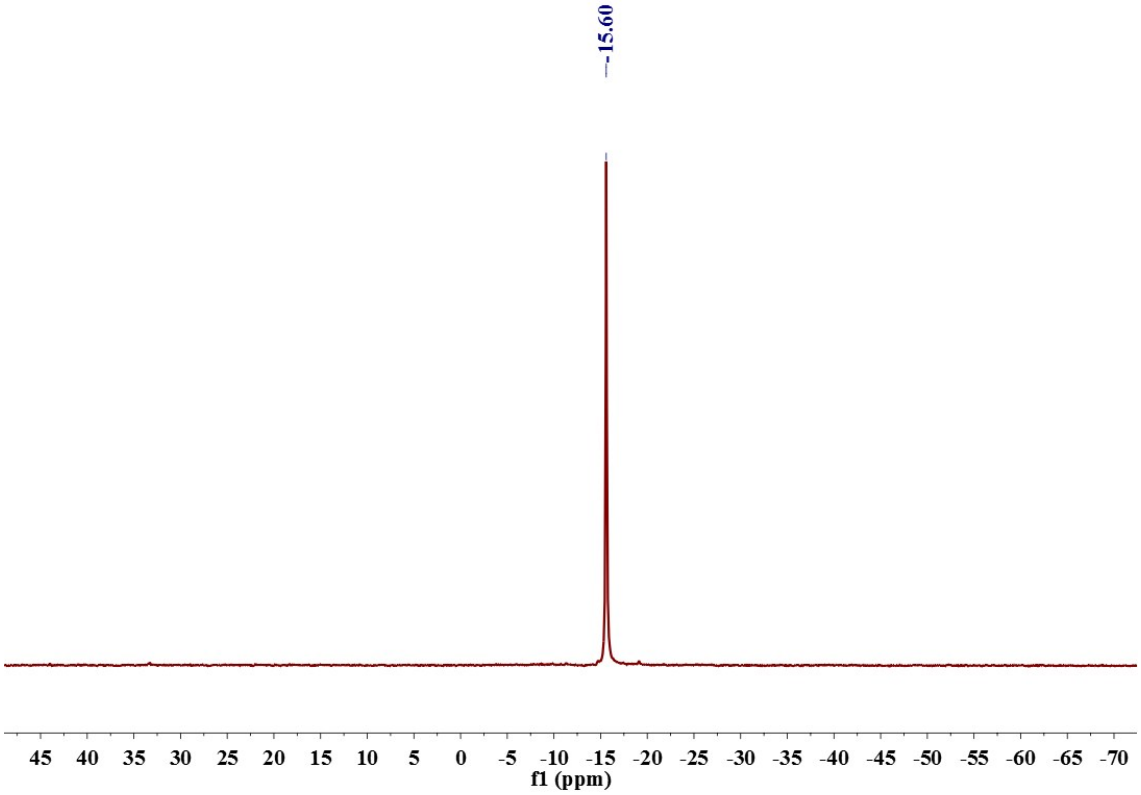

Fig. S4. ^{31}P NMR spectrum of **1** in $CDCl_3$.

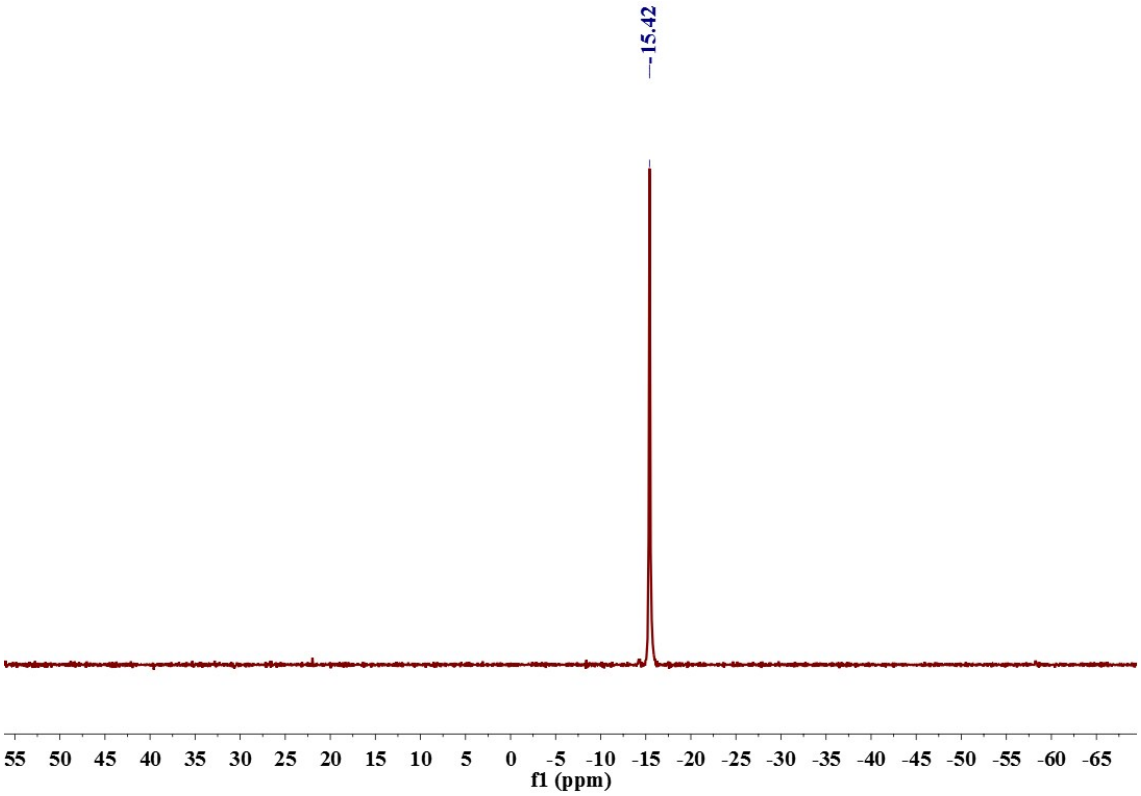

Fig. S5. ^{31}P NMR spectrum of **2** in $CDCl_3$.

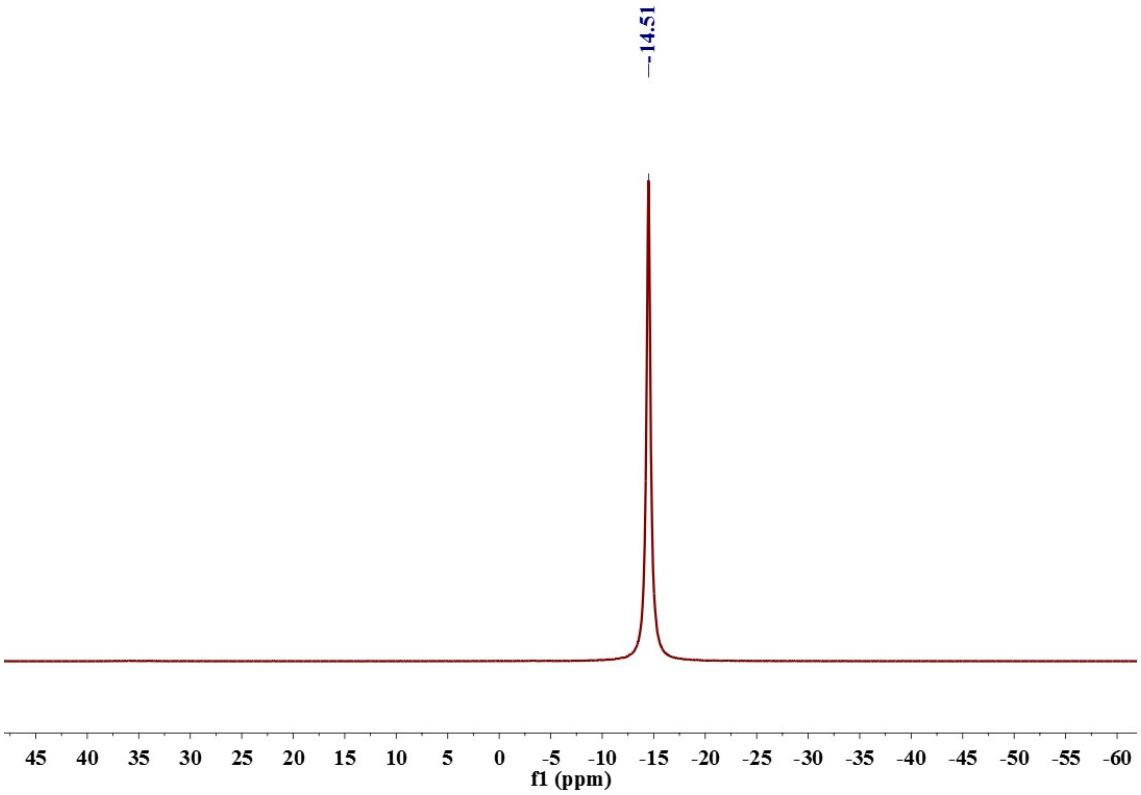

Fig. S6. ^{31}P NMR spectrum of **3** in $CDCl_3$.

2. Molecular structures

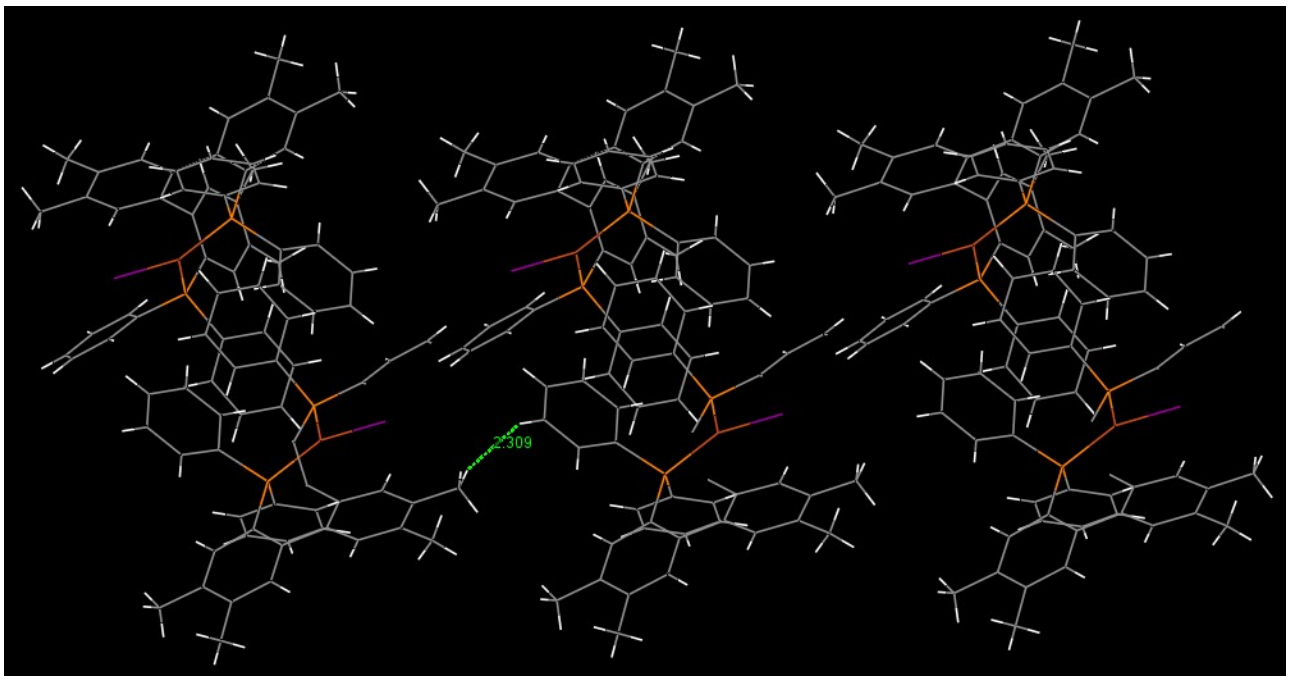

Fig. S7. 1-D molecular structure and C–H···π interactions in **1**.

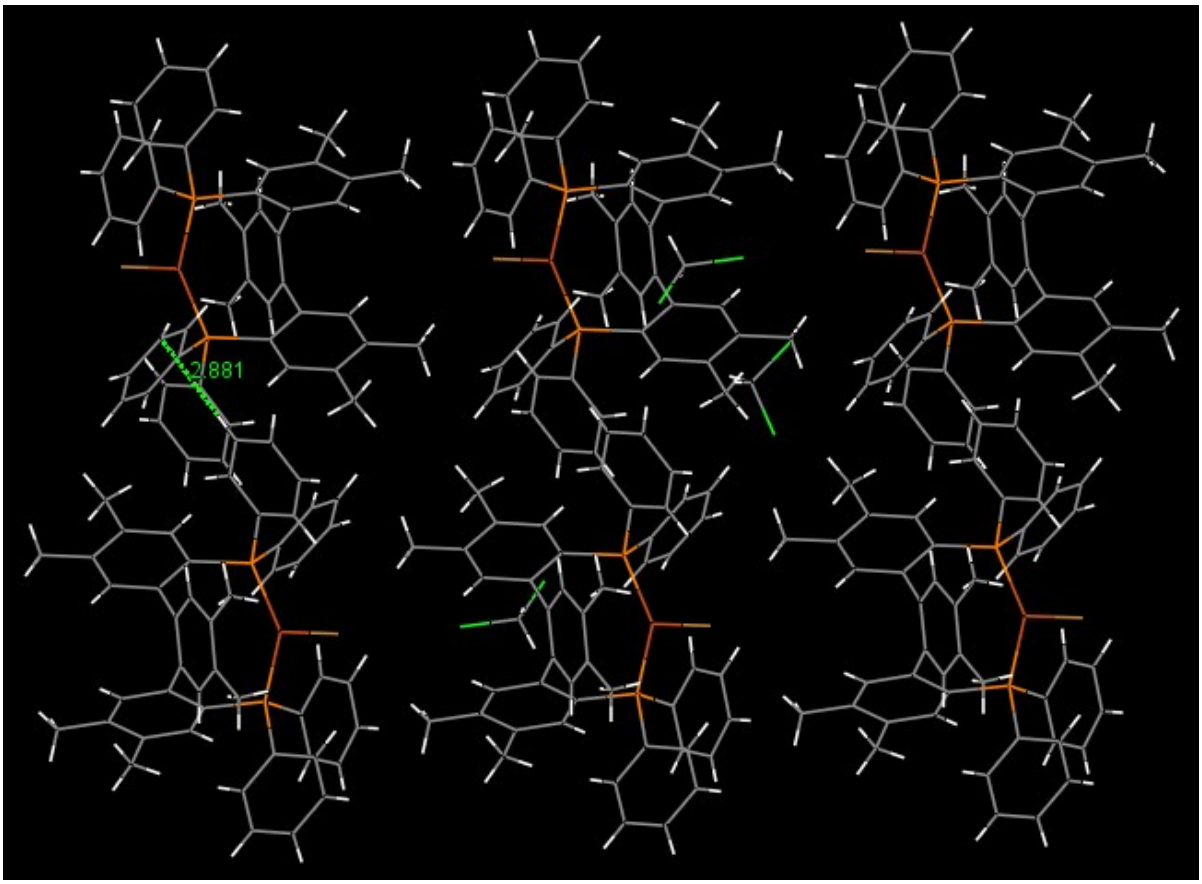

Fig. S8. 1-D molecular structure and C–H···π interactions in **2**.

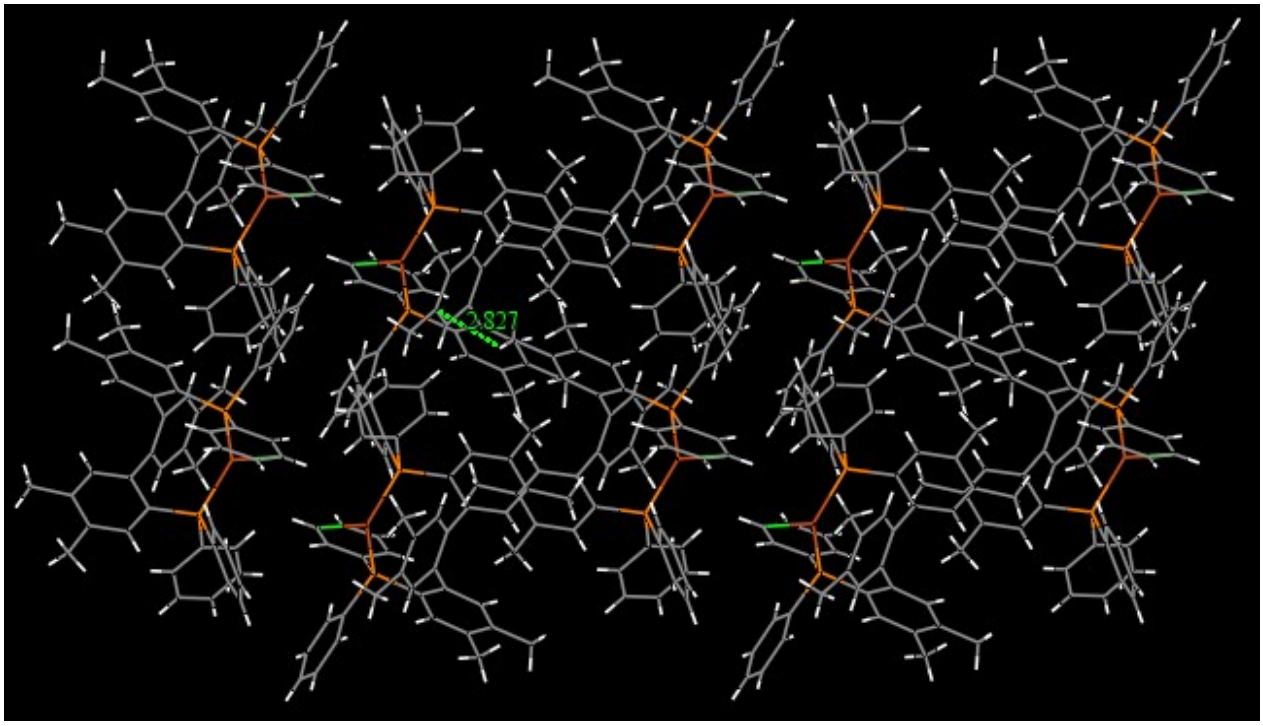

Fig. S9. 1-D molecular structure and C–H···π interactions in **3**.

3. Photophysical properties

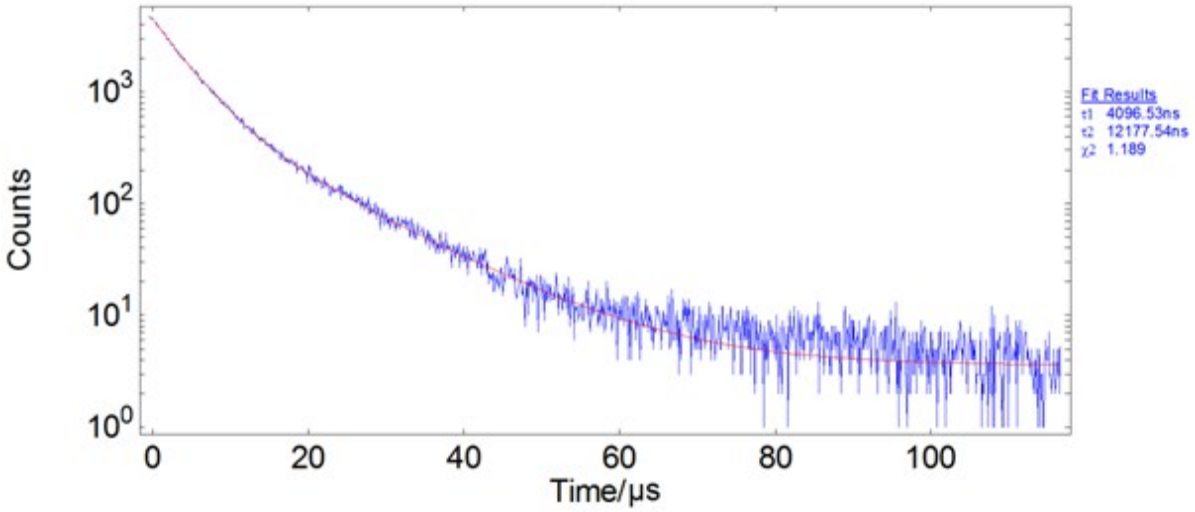

Fit = A + B1.exp(-t/T1) + B2.exp(-t/T2)

	Value	Std Dev		Value	Std Dev	Rel %
T1	4.097E-6	3.935E-8	B1	3.807E+3	2.514E+1	61.29
T2	1.218E-5	1.453E-7	B2	8.089E+2	2.607E+1	38.71
	Chisq	1.189E+0		A	3.593E+0	

Fig. S10. Time profiles of luminescence decay and exponential fit spectrum of **1** at r.t.

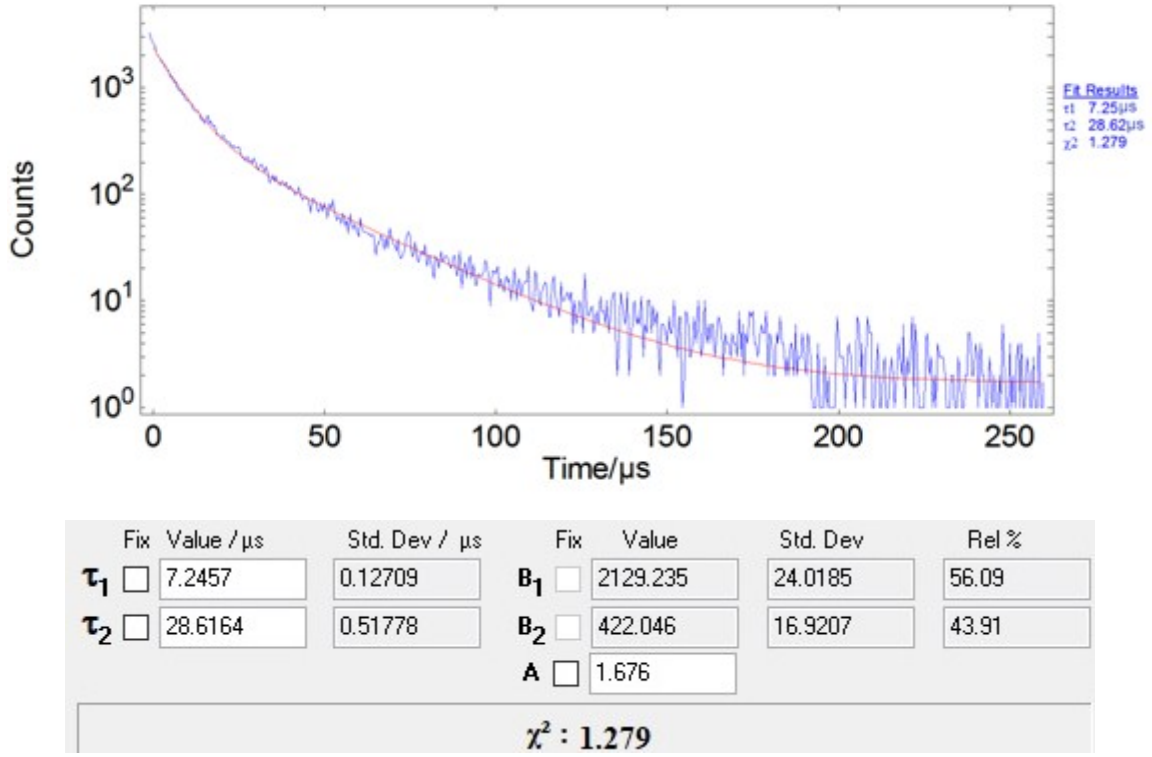

Fig. S11. Time profiles of luminescence decay and exponential fit spectrum of **2** at r.t.

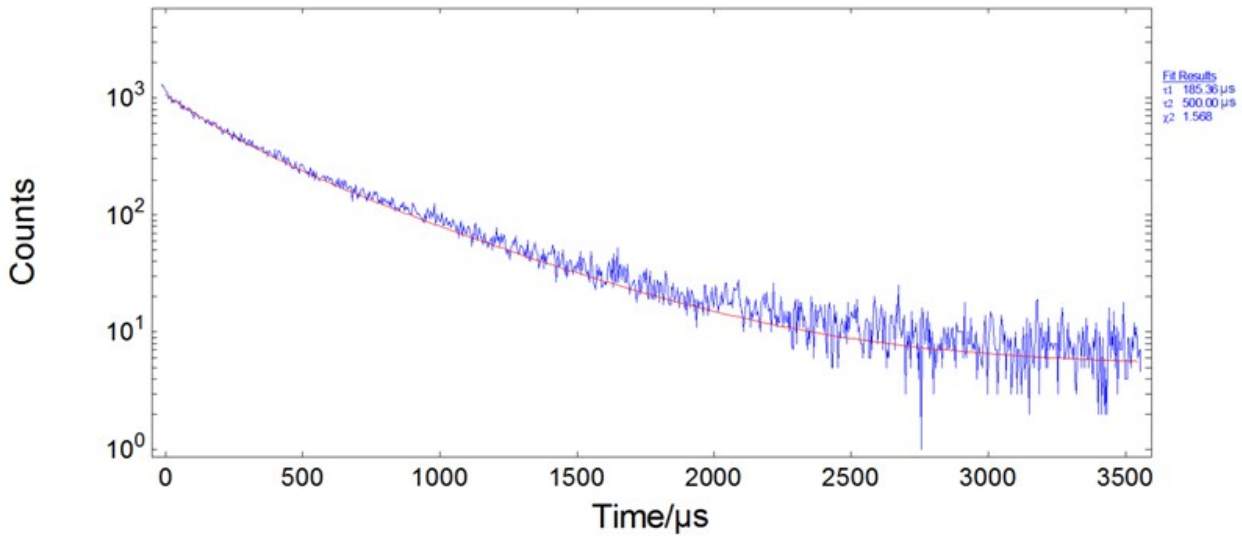

Fit = A + B1.exp(-t/T1) + B2.exp(-t/T2)

	Value	Std Dev		Value	Std Dev	Rel %
T1	1.854E-4	1.019E-5	B1	5.317E+2	2.811E+1	26.73
T2	5.000E-4	1.128E-5	B2	5.404E+2	3.099E+1	73.27
Chisq	1.568E+0		A	5.218E+0		

Fig. S12. Time profiles of luminescence decay and exponential fit spectrum of **3** at r.t.

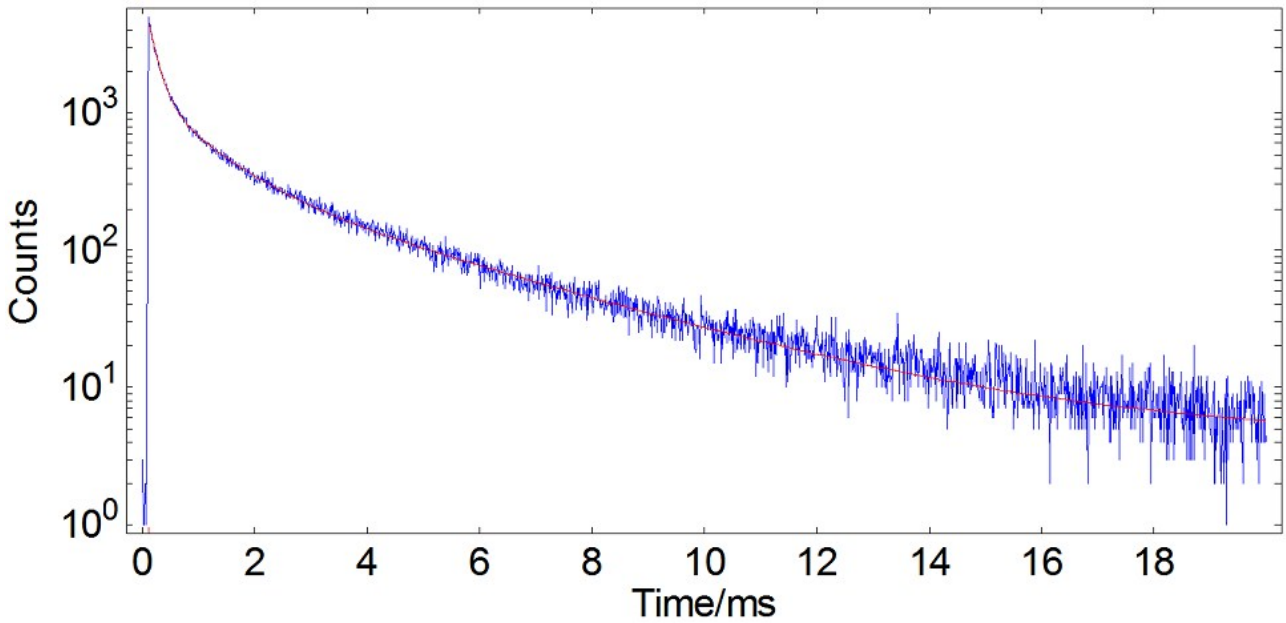

Fit = A + B1.exp(-t/T1) + B2.exp(-t/T2) + B3.exp(-t/T3)

	Value	Std Dev		Value	Std Dev	Rel %
T1	1.687E-4	2.952E-6	B1	3.381E+3	3.411E+1	20.48
T2	9.147E-4	2.634E-5	B2	9.649E+2	2.243E+1	31.68

T3 3.543E-3 5.295E-5 B3 3.761E+2 1.089E+1 47.83

Chisq 1.261E+0 A 4.369E+0

Fig. S13. Time profiles of luminescence decay and exponential fit spectrum of **1** at 77 K.

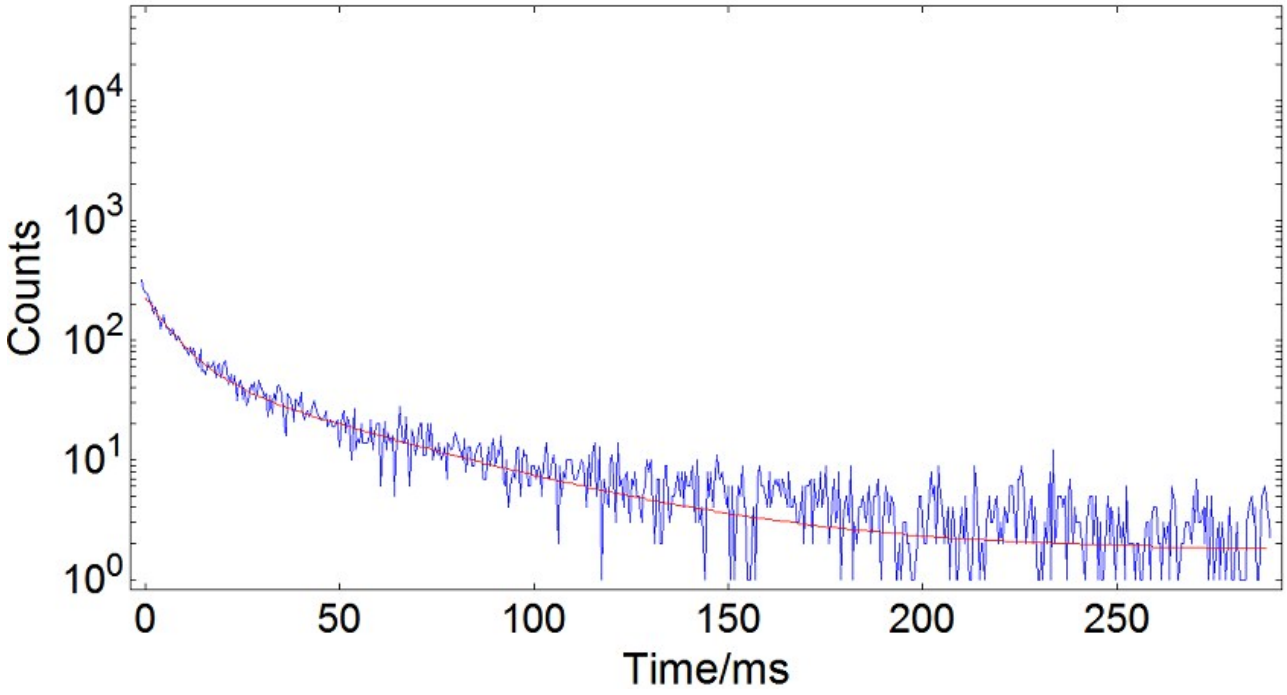

	Fix	Value / ms	Std. Dev / ms		Fix	Value	Std. Dev	Rel %
τ_1	☐	7.3578	0.46404	B_1	☐	180.658	7.3306	34.80
τ_2	☐	43.7401	1.95537	B_2	☐	56.947	3.7293	65.20
				A	☐	1.754		

χ^2 : 1.344

Fig. S14. Time profiles of luminescence decay and exponential fit spectrum of **2** at 77 K.

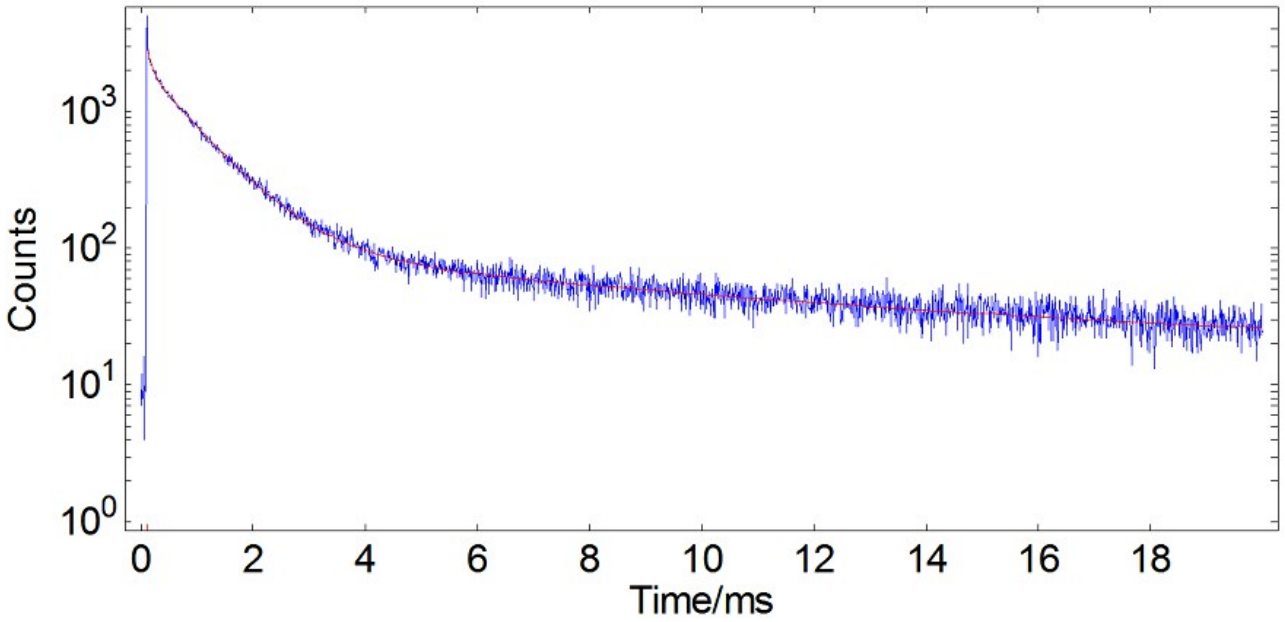

Fit = A + B1.exp(-t/T1) + B2.exp(-t/T2) + B3.exp(-t/T3)

	Value	Std Dev		Value	Std Dev	Rel %
T1	8.197E-5	5.022E-6	B1	1.014E+3	4.000E+1	3.31
T2	8.764E-4	6.587E-6	B2	1.868E+3	1.297E+1	65.16
T3	8.809E-3	5.604E-4	B3	8.995E+1	1.922E+0	31.53
	Chisq	1.239E+0		A	1.670E+1	

Fig. S15. Time profiles of luminescence decay and exponential fit spectrum of **3** at 77 K.

4. Computational details

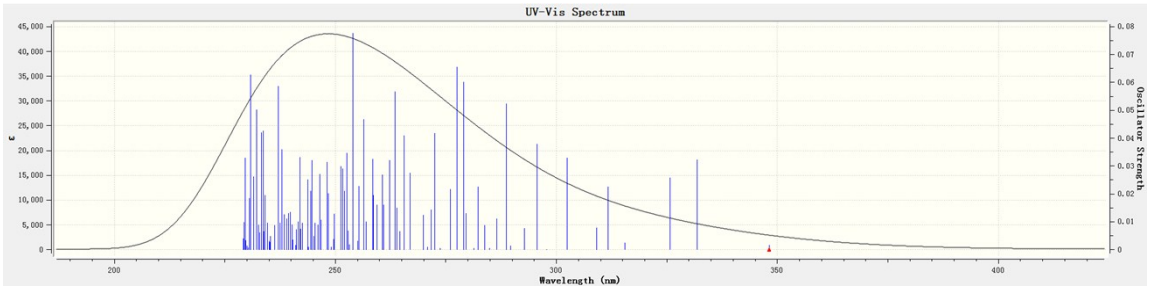

Fig. S16. The absorption spectrum of complex **1** in CH_2Cl_2.

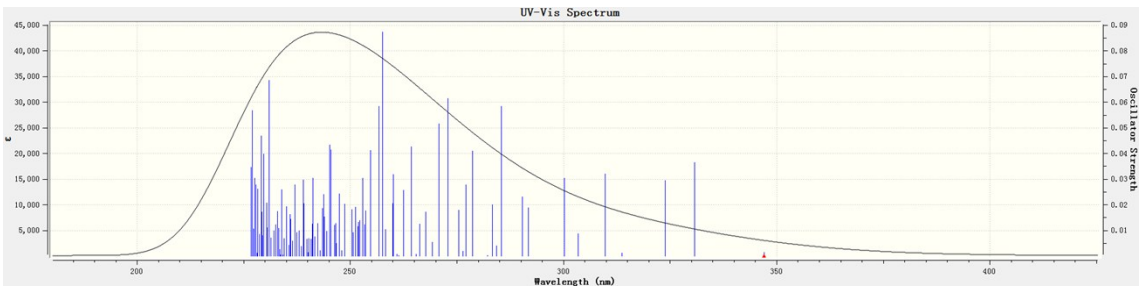

Fig. S17. The absorption spectrum of complex **2** in CH_2Cl_2.

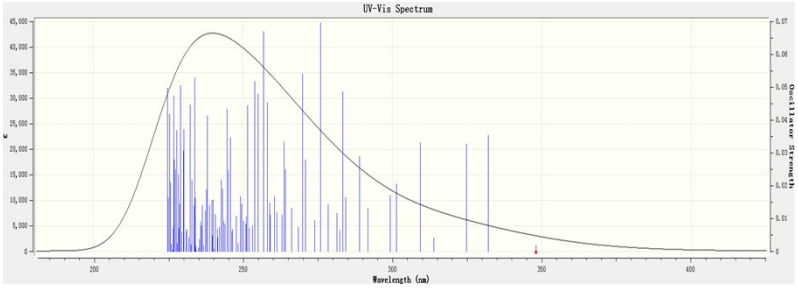

Fig. S18. The absorption spectrum of complex **3** in CH_2Cl_2.

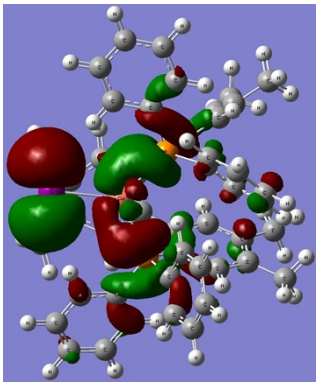

HOMO

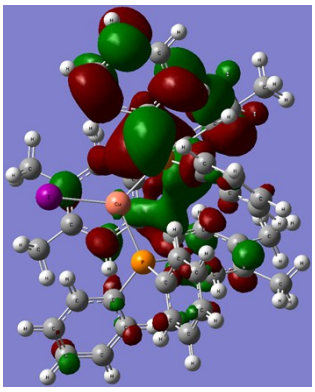

LUMO

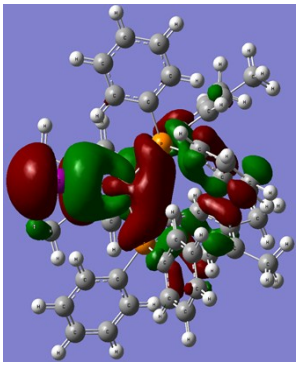

HOMO−1

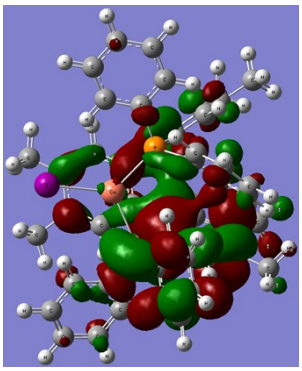

LUMO+1

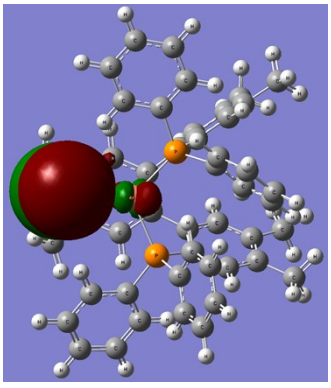

HOMO−2

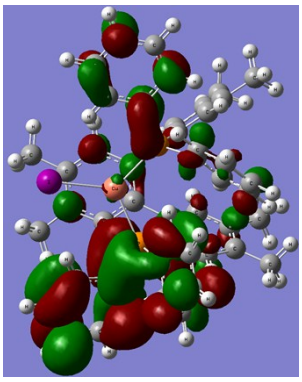

LUMO+2

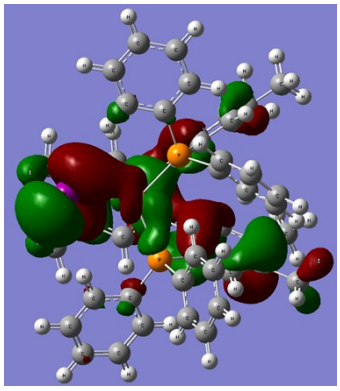

HOMO–3

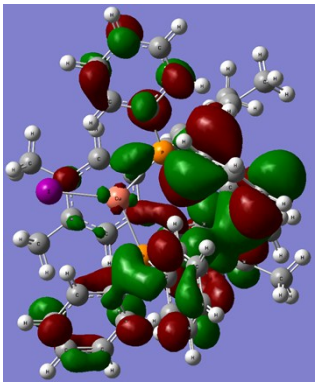

LUMO+3

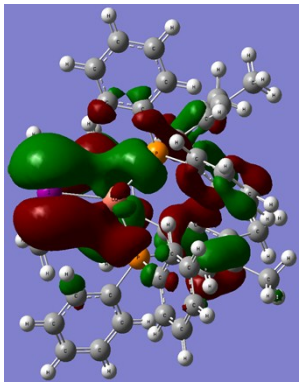

HOMO–4

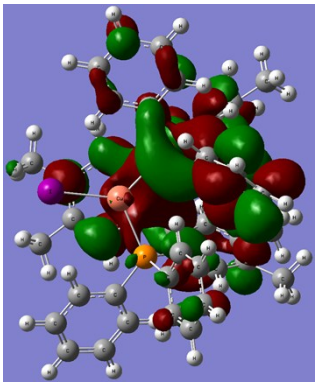

LUMO+4

1

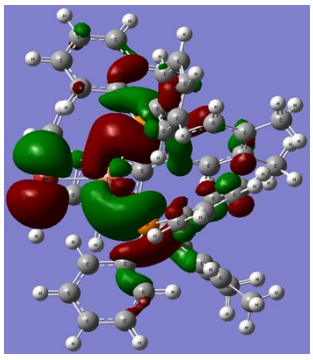

HOMO

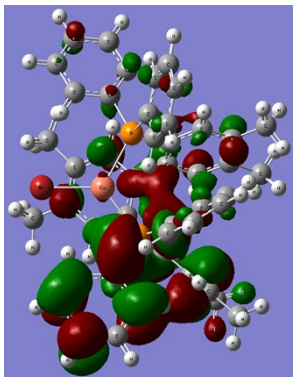

LUMO

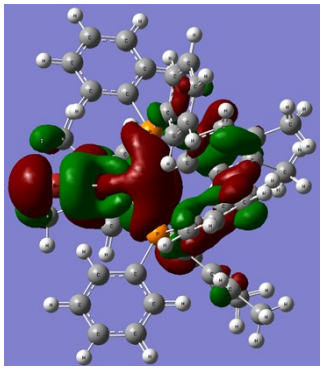

HOMO–1

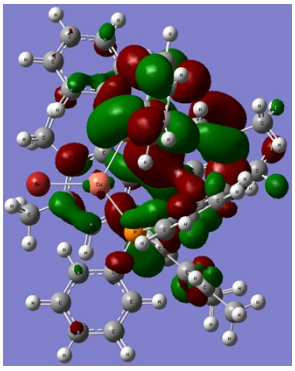

LUMO+1

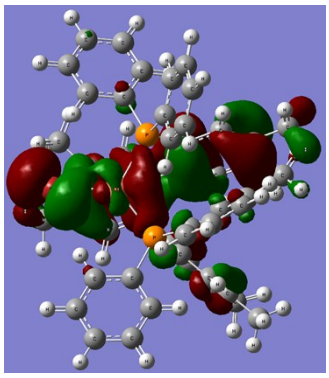

HOMO–2

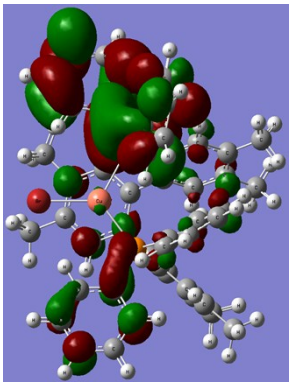

LUMO+2

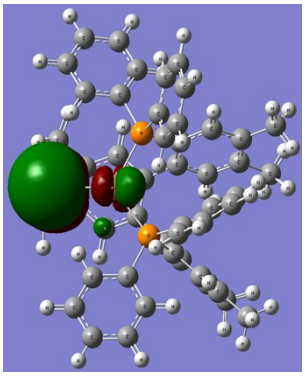

HOMO–3

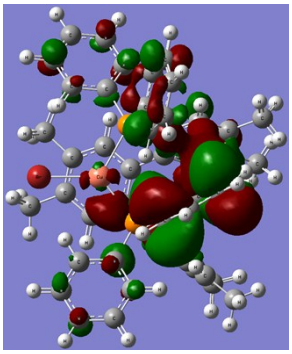

LUMO+3

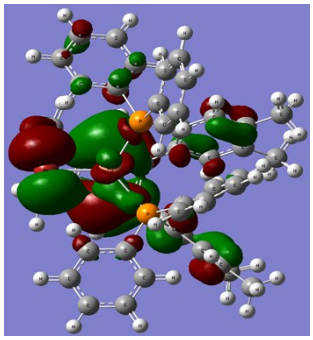

HOMO–4

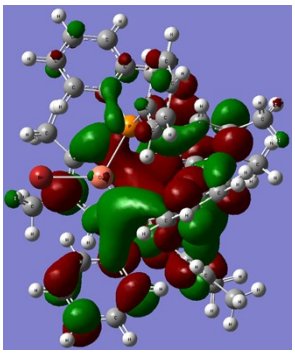

LUMO+4

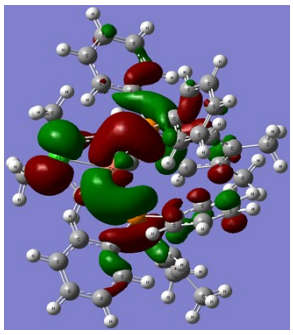

HOMO

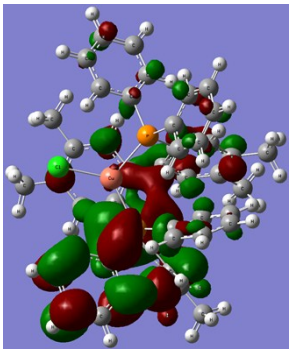

LUMO

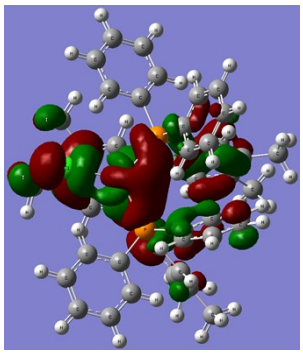

HOMO−1

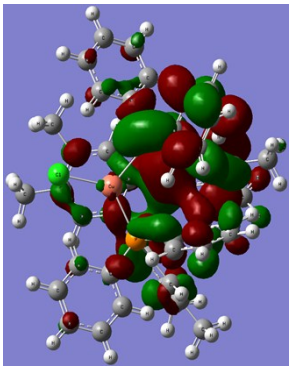

LUMO+1

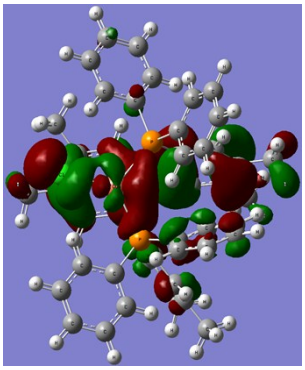

HOMO−2

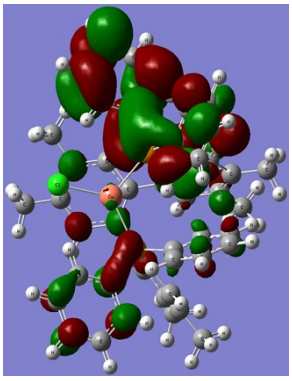

LUMO+2

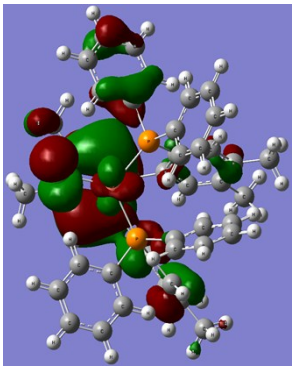

HOMO−3

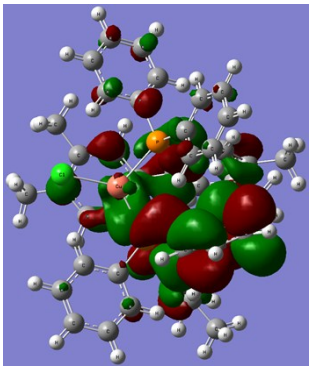

LUMO+3

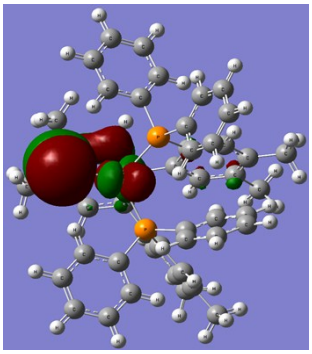

HOMO–4

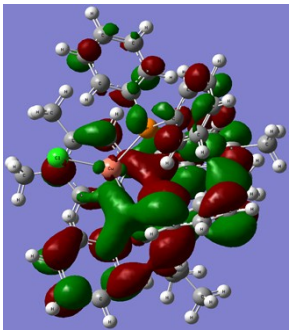

LUMO+4

3

Fig. S19. Contour plots of frontier molecular orbitals of complexes **1-3** in CH_2Cl_2.

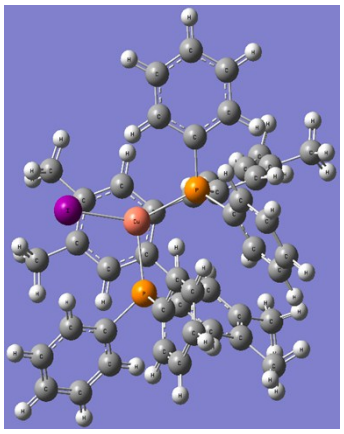

The optimized S_1 geometry

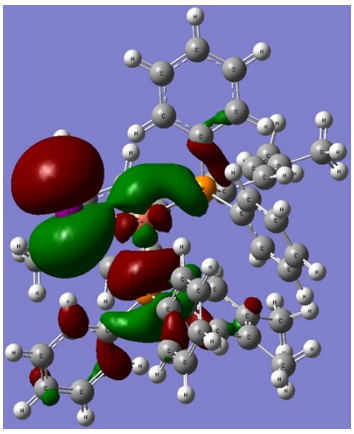

HOMO E = –4.71 eV

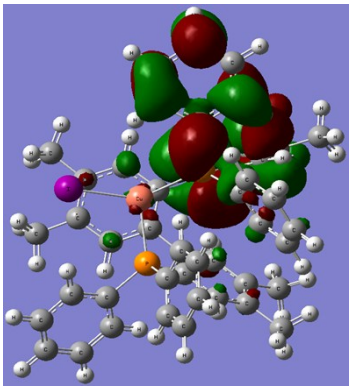

LUMO E = –1.79 eV

1

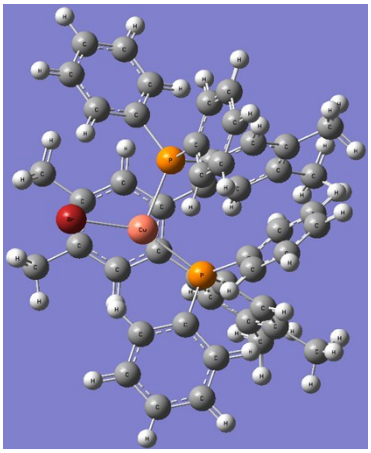

The optimized S_1 geometry

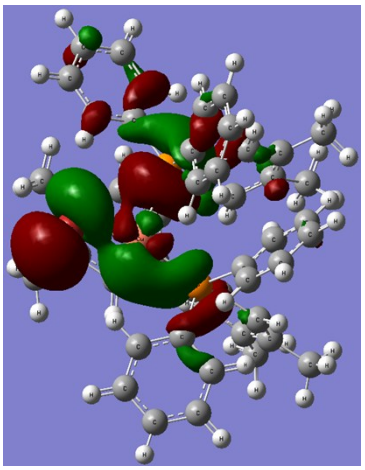

HOMO E = –4.71 eV

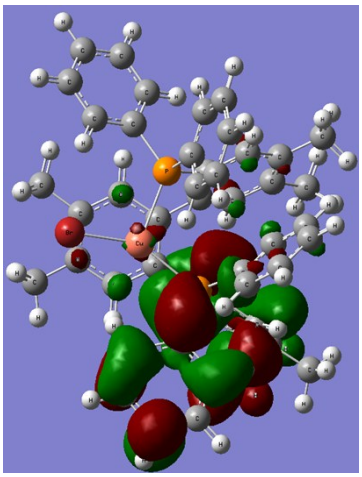

LUMO E = –1.77 eV

2

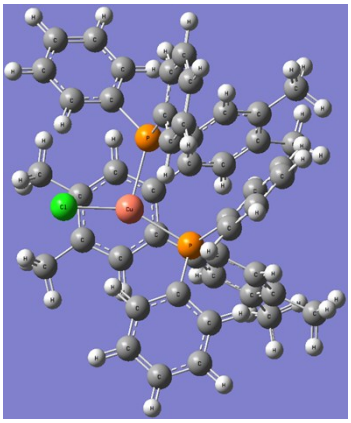

The optimized S_1 geometry

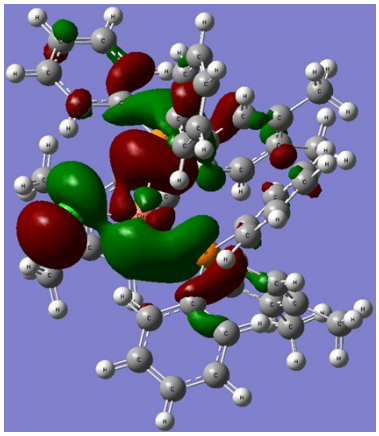

HOMO E = –4.70 eV

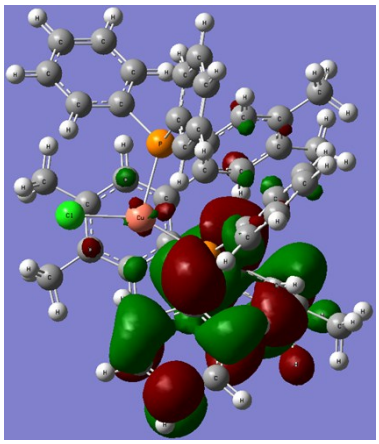

LUMO E = –1.75 eV

3

Fig. S20. The optimized S_1 geometry, electron cloud distribution of HOMO and LUMO at S_1 geometry for complexes **1–3**.

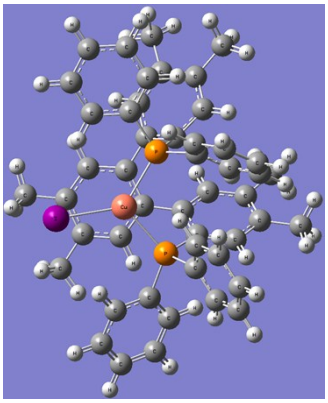

The optimized T_1 geometry

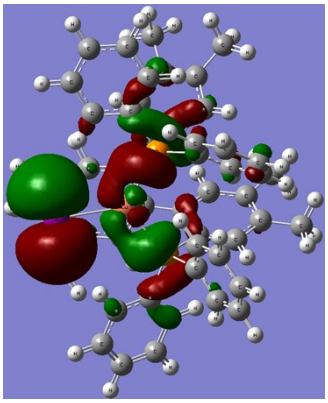

HOMO E = –4.97 eV

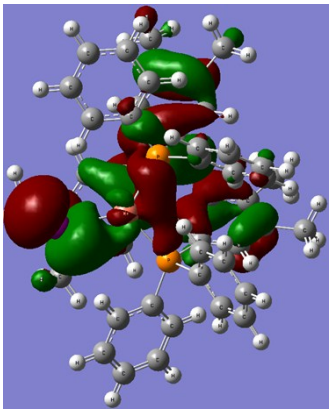

HOMO–2 E = –5.45 eV

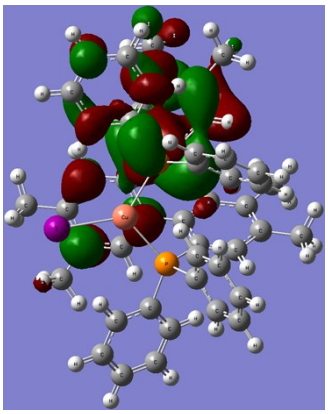

LUMO E = –2.10 eV

1

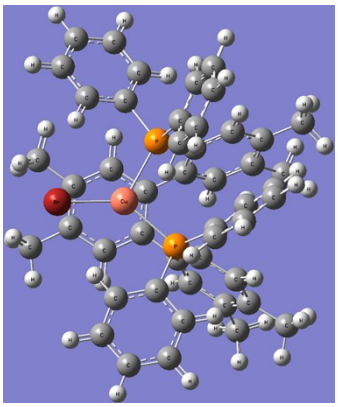

The optimized T_1 geometry

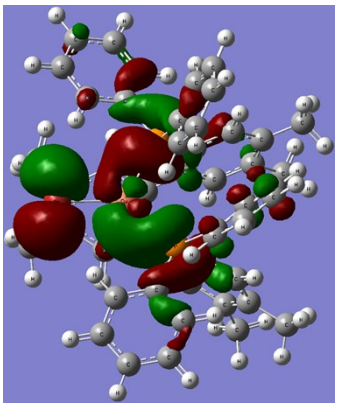

HOMO E = –4.83 eV

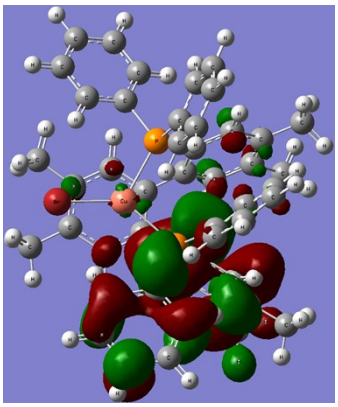

LUMO E = –1.75 eV

2

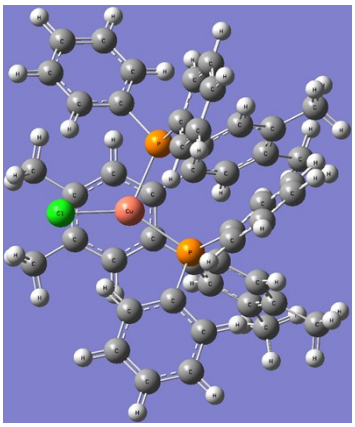

The optimized T_1 geometry

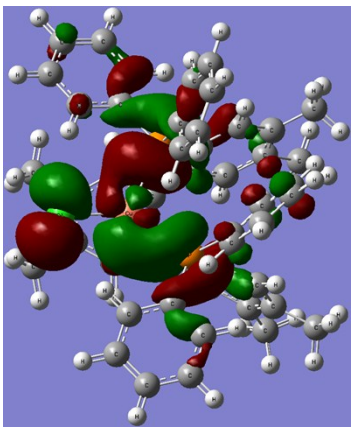

HOMO E = –4.78 eV

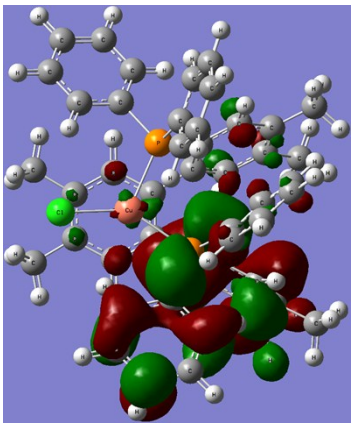

LUMO E = –1.71 eV

3

Fig. S21. The optimized T_1 geometry, electron cloud distribution of HOMO and LUMO at T_1 geometry for complexes **1–3**.

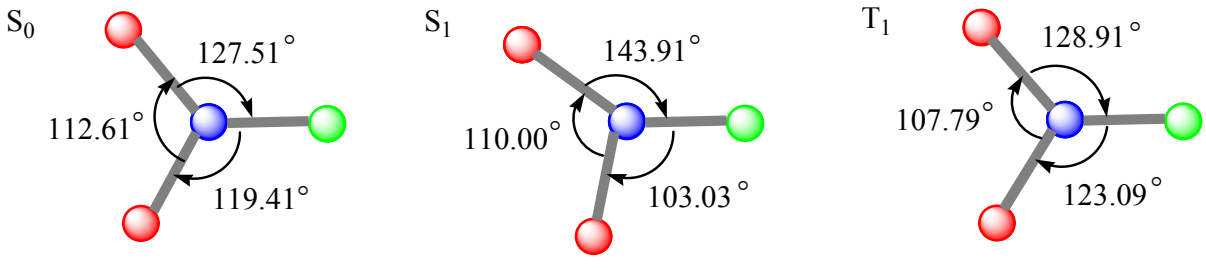

1

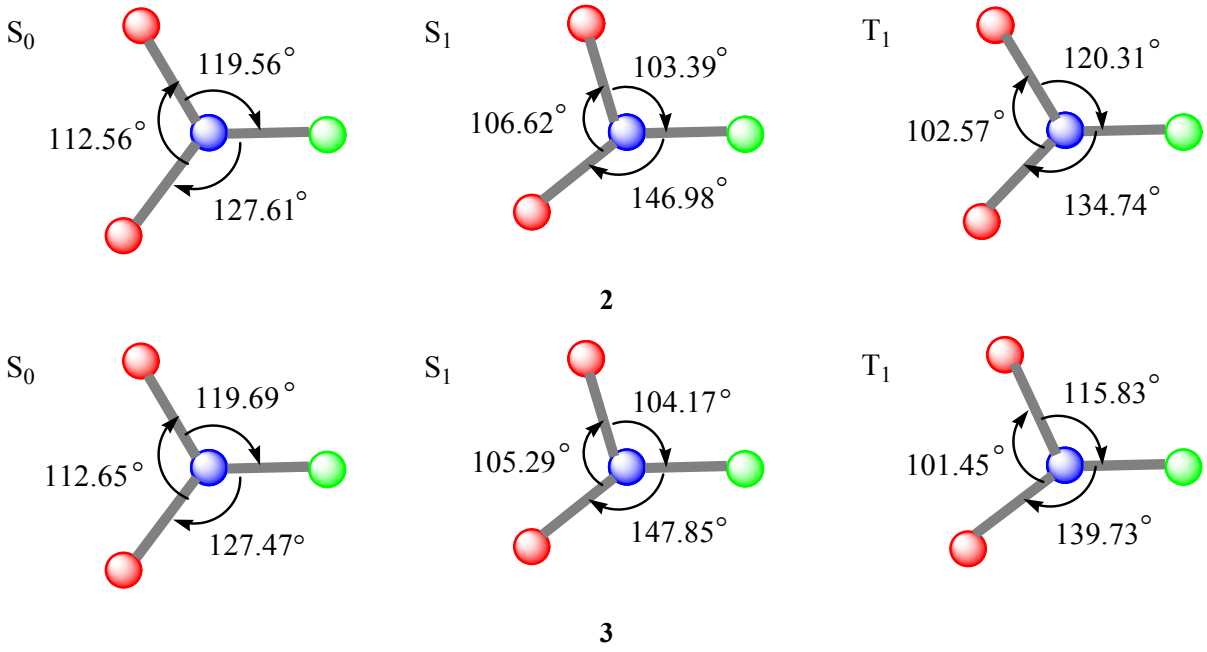

Fig. S22. The core structures in the optimized S_0, S_1, and T_1 geometries for complexes **1-3**.

Table S1. Selected bond lengths (Å) and angles (°) in the optimized S_0, S_1, and T_1 geometries for complexes **1-3**

Complex	Geometry	Cu–X	Cu–P	P–Cu–P	P–Cu–X
1	S_0	2.5742	2.3240, 2.3227	112.61	127.51, 119.41
	S_1	2.5346	2.3360, 2.3569	110.00	143.91, 103.03
	T_1	2.5580	2.3320, 2.3222	107.79	128.91, 123.09
2	S_0	2.3915	2.3159, 2.3171	112.56	119.56, 127.61
	S_1	2.3286	2.3605, 2.3374	106.62	103.39, 146.98
	T_1	2.3398	2.3261, 2.3330	102.57	120.31, 134.74
3	S_0	2.2708	2.3092, 2.3073	112.65	127.47, 119.69
	S_1	2.2069	2.3398, 2.3643	105.29	147.85, 104.17
	T_1	2.2222	2.3238, 2.3339	101.45	139.73, 115.83

Table S2. Computed excitation states for complex **1** in CH_2Cl_2.

State	λ(nm)/*E*(eV)	Configurations	*f*
1	348.2 (3.56)	H→L(98)	0.0016
12	288.7 (4.29)	H-3→L (81); H-1→L+1 (4) ; H-1→L+2 (6)	0.0523
19	279.0 (4.44)	H-3→L+1 (17); H-1→L+3 (35); H-1→L+4 (25); H→L+9 (12)	0.0602
20	277.5 (4.47)	H-3→L+1 (54); H-3→L+2 (4); H-1→L+3 (12);	0.0656

		H-1→L+5 (2); H→L+9 (15); H→L+10 (3)	
31	263.4 (4.71)	H-6→L (3); H-4→L+1 (15); H-3→L+4 (50);	0.0567
		H-2→L+5 (11); H→L+12 (6)	
42	254.0 (4.88)	H-7→L (48); H-5→L (4); H-5→L+1 (11);H-5→L+4 (2);	0.0775
		H-3→L+6 (3); H-1→L+9 (5); H→L+11 (3)	
		H-10→L (6); H-10→L+1 (4); H-8→L+3 (4); H-8→L+4 (2);	
78	237.1 (5.23)	H-7→L+2 (12); H-6→L+2 (3); H-6→L+3 (25); H-6→L+4 (7);	0.0586
		H-5→L+2 (2); H-5→L+4 (2); H-4→L+7 (4); H-3→L+9 (2)	
		H-15→L (5); H-14→L (3); H-11→L (4); H-10→L+1 (4);	
91	232.1 (5.34)	H-9→L+1 (5); H-8→L+3 (24); H-7→L+3 (3);	0.0501
		H-5→L+6 (3); H-4→L+8 (9); H-3→L+10 (3);	
		H-3→L+12 (2); H-1→L+13 (6); H-1→L+14 (5)	
		H-15→L (6); H-14→L (6); H-13→L (2); H-9→L+1 (5);	
93	230.8 (5.37)	H-8→L+3 (26); H-8→L+4 (11); H-7→L+3 (3); H-7→L+4 (5);	0.0628
		H-6→L+3 (5); H-6→L+5 (2); H-5→L+6 (3)	

Table S3. Computed excitation states for complex **2** in CH_2Cl_2.

State	λ(nm)/*E*(eV)	Configurations	*f*
1	347.1 (3.57)	H→L (98)	0.0015
10	285.4 (4.34)	H-2→L (71); H-1→L+1 (15); H→L+7 (2)	0.0585
18	272.9 (4.54)	H-1→L+3 (90)	0.0614
19	270.8 (4.58)	H-2→L+1 (5); H-2→L+2 (2); H→L+10 (85)	0.0516
31	257.5 (4.81)	H-4→L+1 (41); H-3→L+4 (5); H-2→L+4 (10);	0.0815
		H-1→L+8 (5); H→L+11 (10); H→L+12 (9)	
32	256.7 (4.83)	H-6→L (60); H-3→L+4 (9); H-2→L+3 (8); H-1→L+6 (5)	0.0585
		H-10→L+1 (12); H-9→L+1 (6); H-9→L+2 (3);	
86	230.9 (5.37)	H-8→L+3 (13); H-7→L+3 (2); H-7→L+4 (3);	0.0685
		H-6→L+6 (3); H-5→L+5 (12); H-2→L+10 (15)	
99	227.0 (5.46)	H-19→L (16); H-16→L (6); H-15→L (11); H-11→L+3 (3);	0.0567
		H-9→L+4 (4); H-7→L+3 (4); H-7→L+5 (5); H-6→L+6 (6)	

Table S4. Computed excitation states for complex **3** in CH_2Cl_2.

State	λ(nm)/*E*(eV)	Configurations	*f*
1	348.1 (3.56)	H→L(98)	0.0018
15	276.0 (4.49)	H-2→L+1 (33); H-2→L+4 (2); H-1→L+3 (22);	0.0697
		H-1→L+4 (16); H→L+9 (14)	
18	270.1 (4.59)	H-1→L+3 (35); H-1→L+4 (54); H→L+10 (3)	0.0541
29	256.9 (4.83)	H-4→L+1 (6); H-3→L+1 (51); H-3→L+2 (3) ; H-2→L+4 (12);	0.0670
		H-1→L+6 (4); H-1→L+8 (2); H→L+12 (2)	
31	254.0 (4.88)	H-6→L (20); H-5→L (4); H-5→L+1 (3);	0.0518
		H-4→L+1 (46); H-4→L+2 (5)	

74	233.9 (5.30)	H-14→L (3); H-9→L+1 (3); H-8→L+1 (3); H-8→L+2 (5); H-7→L+3 (17); H-6→L+3 (11); H-6→L+4 (14); H-4→L+5 (7); H-3→L+5 (5); H-2→L+10 (2); H-1→L+11 (6)	0.0529
85	229.1 (5.41)	H-13→L (4); H-13→L+1 (4); H-12→L+1 (5); H-11→L+1 (15); H-10→L+1 (2); H-10→L+2 (3);H-5→L+5 (26); H-5→L+6 (3); H-4→L+6 (4);H-3→L+8 (3)	0.0505

Table S5. Calculated emission wavelength (λ), oscillator strength (f) and main configuration of complexes **1-3** along with their experimental values ($\lambda_{expt.}$).

Complex	λ (nm)	f	Main configurations	$\lambda_{expt.}$ (nm)
1	528	0.0005	HOMO→LUMO (99%)	493
2	537	0.0005	HOMO→LUMO (99%)	527
3	541	0.0141	HOMO→LUMO (99%)	533

Table S6. Calculated vertical excitation energies of singlet and triplet excited states as well as the energy gap of complexes **1-3** at the X-ray structure, the optimized S_0, S_1 and T_1 geometries.

Complex	Geometry	Excitation energies (eV)		Energy gap (eV)
		S_1	T_1	$\Delta E(S_1\text{-}T_1)$
1	X-ray	3.2061	3.1451	0.0610
	S_0	3.1512	3.0904	0.0608
	S_1	2.3464	2.3042	0.0422
	T_1	2.2703	1.5333	0.7370
2	X-ray	3.4110	3.2762	0.1348
	S_0	3.2604	3.1660	0.0944
	S_1	2.3093	2.2486	0.0607
	T_1	2.4119	2.2834	0.1285
3	X-ray	3.4024	3.2859	0.1165
	S_0	3.3046	3.1889	0.1157
	S_1	2.2929	2.2232	0.0697
	T_1	2.3870	2.2707	0.1163